
A WT-RESNET BASED FAULT DIAGNOSIS MODEL FOR THE URBAN RAIL TRAIN TRANSMISSION SYSTEM

A PREPRINT

Zuyu Cheng

School of Mechanical Engineering
Xi'an Jiaotong University
Xi'an 710049, China

Zhengcai Zhao

School of Mechanical Engineering
Xi'an Jiaotong University
Xi'an 710049, China

Yixiao Wang

School of Mechanical Engineering
Xi'an Jiaotong University
Xi'an 710049, China

Wentao Guo

School of Mechanical Engineering
Xi'an Jiaotong University
Xi'an 710049, China

Yufei Wang

School of Mechanical Engineering
Xi'an Jiaotong University
Xi'an 710049, China

Xiang Gao

School of Mechanical Engineering
Xi'an Jiaotong University
Xi'an 710049, China

June 11, 2024

ABSTRACT

This study presents a novel fault diagnosis model for urban rail transit systems based on Wavelet Transform Residual Neural Network (WT-ResNet). The model integrates the advantages of wavelet transform for feature extraction and ResNet for pattern recognition, offering enhanced diagnostic accuracy and robustness. Experimental results demonstrate the effectiveness of the proposed model in identifying faults in urban rail trains, paving the way for improved maintenance strategies and reduced downtime.

Keywords Wavelet Transform · ResNet · Fault Diagnosis · Urban Rail Transit · Machine Learning

1 Introduction

In March 2021 at the meeting of the Commission for Financial and Economic Affairs under the CPC Central Committee, Carbon peaking and neutrality were seriously taken account of and incorporated into the overall plan of China for environment protection, which has proposed higher demand of the quantity and quality of urban railway system. The progression of urban railway system are reflected in the safety and reliability of transportation vehicles. Therefore, ensuring the normal operation of these vehicles has emerged as a crucial issue confronting the current development. Under the circumstances, the conventional methods and modes of the operations and maintenance of vehicles are no longer adequate to meet the current demand that they have to operate with high efficiency, rigorous standardization and precise refinement.[He et al. [2020]]

The conventional method of operations and maintenance entails conducting maintenance activities only upon the detection of a fault in the mechanical equipment, which is called “fireman” as they just can come in handy after the accidents happened, putting the operations and maintenance in a passive state [Yang [2018]]. Gradually, a method of regular diagnosis emerged, which involves assessing the operational status of mechanical equipment periodically to determine whether the maintenance is required or not. However, it faces issues related to timeliness, as guaranteeing the timely detection and resolution of faults is definitely a tough work. It's common to miss the accident when adopting the regular diagnosis pattern.

The advancement of modern information technology and artificial intelligence (AI), exemplified by technologies like big data analysis, machine learning, and deep learning algorithms, has led to the emergence of intelligent operations and maintenance as a highly effective approach for equipment upkeep. By employing methodologies such as data mining, association analysis, and trend analysis, the development of an intelligent operation and maintenance system

for equipment is facilitated. This system offers sophisticated features such as remote monitoring, fault detection, expert diagnosis, health management, and other intelligent functionalities, which serve to improve the efficiency, accuracy, reliability, and versatility of operation and maintenance processes, while simultaneously reducing labor costs and minimizing operational errors [Peng et al. [2019]].

Intelligent fault diagnosis is an essential part of intelligent operation and maintenance, which has made great, advanced progress and achievements with the development of AI. The traditional machine learning methods, such as support vector machine(SVM) and artificial neural network(ANN), have been widely used in fault diagnosis, but they have limited ability to process natural data and rely to much on the expertise in some specific area. Presently, deep learning(DL) has been widely used and made tremendous contributions to the fault diagnosis technology. DL theory was first published in Science in 2006 by Hinton et al[Hinton and Salakhutdinov [2006]] .It performs outstandingly in discovering intricate structures in high-dimensional data[LeCun et al. [2015]] , which is beneficial to some classification or detection tasks, hence, DL is utilized widely in industry and science. DL methods, such as stacked self-encoders(SAE), convolutional neural network(CNN) and recurrent neural network(RNN), are studied and used widely in fault diagnosis. SAE is a type of artificial neural network used for unsupervised learning. It consists of multiple layers of autoencoders, where each layer learns to encode the input data and reconstruct it at the output. Trained layer by layer using some techniques like backpropagation, SAE can perform well in the tasks like feature learning and dimensionality reduction. CNN is a supervised learning network, aiming to learn spatial hierarchies of features from input data automatically. It consists of diverse layers, including convolutional layers, pooling layers, and fully connected layers, and are very useful in facial recognition and autonomous vehicles. RNN is designed for process sequential data by retaining the previous inputs. A fundamental aspect of RNN is their capability to discern dependencies and patterns within sequential data through the context of preceding inputs. Based on its features, RNN is commonly used in machine translation, natural language and time series analysis.

DL has progressed greatly these years, the residual neural network(ResNet) is one of the achievements. ResNet was first proposed by Kaiming He et al. to address the degradation problem[He et al. [2016a]] , which made it easier to train deeper neural networks and optimize them. It's better for ResNet to converge more easily when trained, helping reduce the time cost for training process. Moreover, ResNet performed well in generalization ability, allowing it to adapt to multiple sets of data and tasks while performing outstandingly in terms of accuracy and efficiency. In this article, we utilize the ResNet to construct the system of diagnosis and analyze its performance.

2 Theoretical foundation

2.1 Convolutional neural networks

Convolutional Neural Network(CNN) was first proposed by LeCun and initially applied to image recognition. Due to the characteristics of local receptive fields, shared weights, and spatial subsampling, CNN has been successfully applied in various fields such as document recognition, speech recognition, spectrum recognition, and fault diagnosis[Lecun et al. [1998]].The structure of CNN typically consists of multiple alternating convolutional layers, pooling layers, and fully connected layers. The convolutional and pooling layers are responsible for extracting features layer by layer, while the fully connected layers are responsible for feature classification or regression. A typical CNN structure is shown in Figure 1.

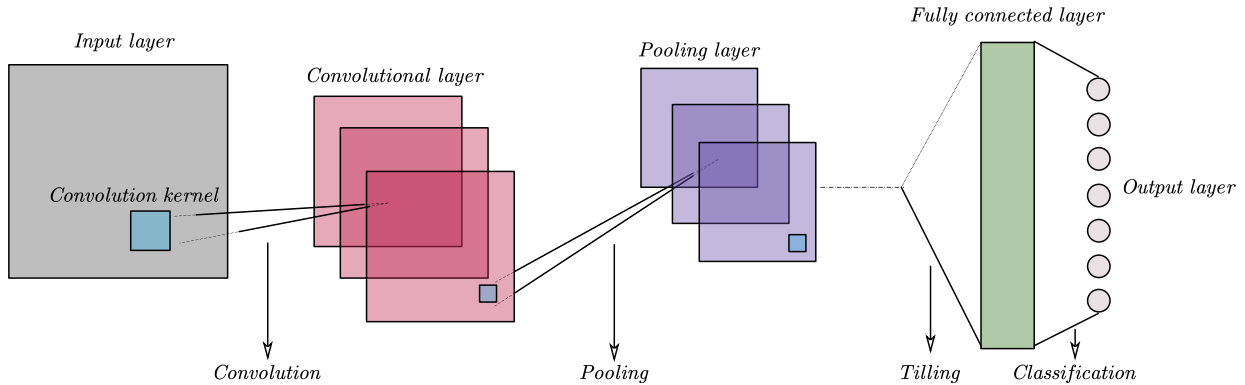


Figure 1: Convolutional neural network structure diagram

Convolutional Layer: The convolutional layer plays a crucial role in the feature extraction process by applying convolution operations to the input or the features from the preceding layer to generate fresh features that serve as the input for the subsequent layer. This operation is underpinned by the convolutional kernel filter, which is instrumental in capturing the local features present within the input data. By sliding across the input data, the filter produces a series of outputs, known as feature maps, where each position corresponds to a different feature activation. The convolutional kernel filter functions as a shared weight mechanism, linking the current layer to the next layer, a concept referred to as weight sharing. Subsequent to the convolution operation, a non-linear activation function is applied to the resulting feature map to augment its expressiveness. This entire convolutional process is mathematically encapsulated in formula 1, which formalizes the transformation of the input data into a more abstract feature representation.

$$X_k^l = \phi \left(\sum_{k=1}^K W_k^l * X_k^{l-1} + B_k^l \right) \quad (1)$$

Here, X_k^l represents the k -th output of convolutional layer l , where k denotes the number of convolutional kernels in layer l , W_k^l represents the k -th convolutional kernel of layer l , $*$ denotes convolution operation, X_k^{l-1} represents the k -th output of the layer $l-1$, B_k^l represents the bias of convolutional layer l , ϕ represents the non-linear activation function applied to the convolution output. Non-linear activation functions can map features to non-linear spaces, thereby enhancing the linear separability of features. Common non-linear activation functions include the Sigmoid function, Tanh function, ReLU function, etc.

Pooling Layer: Positioned following the convolutional layer, the pooling layer serves a dual purpose: it not only distills the essential local information from the extracted features but also reduces the dimensionality of these features, thereby decreasing the computational demand associated with the subsequent parameter updates. Among the available pooling techniques, max pooling stands out as the predominant choice due to its ability to select the maximum value within a specified region, as mathematically expressed in equation 2, which effectively captures the most prominent feature within that area.

$$P_{ijk}^l = \max (x_{ijk}^l : i \leq i < i + p, j \leq j < j + q) \quad (2)$$

Here, P_{ijk}^l represents the output of pooling layer l , x_{ijk}^l represents the (i, j) element in the k -th feature map output by convolutional layer l , and p and q respectively represent the length and width of the pooling window.

Fully connected layer: Once the input data has undergone the initial processing steps of convolutional and pooling layers to extract relevant features, it enters the fully connected layer where these features are transformed into a one-dimensional form suitable for classification. This layer typically consists of several hidden layers, culminating in an output layer that performs the actual classification. The output layer often employs the Softmax function to convert raw scores into probabilities, with each class probability computed using the formula shown in equation 3, thus completing the classification process.

$$O_j = O_j = \begin{bmatrix} P(y = 1/x; \theta) \\ P(y = 2/x; \theta) \\ \dots \\ P(y = k/x; \theta) \end{bmatrix} = \frac{1}{\sum_{j=1}^k \exp(\theta^j x)} \begin{bmatrix} \exp(\theta^1 x) \\ \exp(\theta^2 x) \\ \dots \\ \exp(\theta^k x) \end{bmatrix} \quad (3)$$

Where k represents the number of categories, and $\exp(\theta^j x)$ represents the parameters of the classification layer.

2.2 The residual network

In 2016, He et al. made a breakthrough in deep learning by introducing the Residual Neural Network (ResNet)[He et al. [2016b]], which was designed to overcome challenges such as model degradation and overfitting that often arise in deeper neural network models. ResNet's innovative approach involves the use of residual blocks that facilitate the learning of residual features, thereby enhancing the flow of information through the network. This groundbreaking architecture achieved remarkable success in the ImageNet image recognition competition, setting new standards in the field of computer vision. Meanwhile, other notable neural network models, such as AlexNet[Krizhevsky et al. [2012]], GoogLeNet, and VGGNet[Russakovsky et al. [2014]], had already made significant impacts in the early to mid-2010s, but they were generally considered shallow network models. These models, while successful in their own right, faced

limitations when attempting to scale to greater depths. Residual neural networks introduced the concept of residual learning, learning residual features through multiple connected residual blocks, as shown in Figure 2.

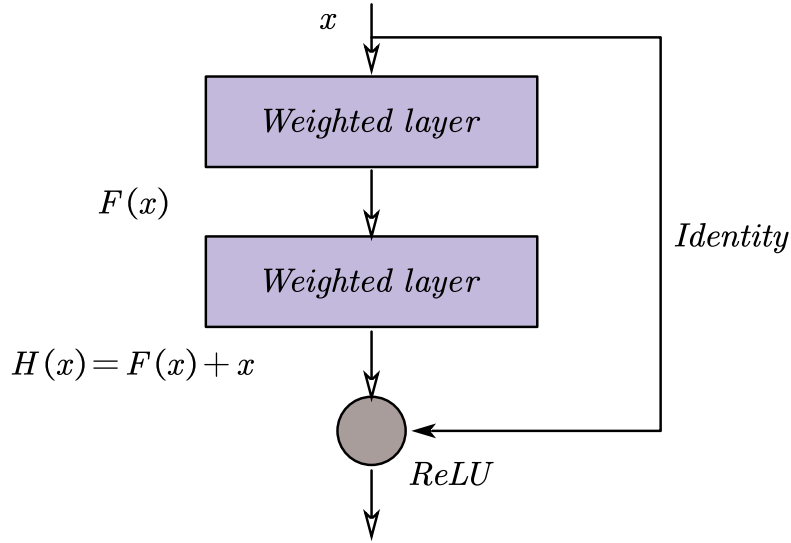


Figure 2: Structure diagram of the residual block

Here, x is the input of the residual neural network, $H(x)$ is the output, $F(x)$ is the residual mapping function. $H(x) = F(x, \{W_i\}) + x$ is the identity mapping function, and the *Weightlayer* is the convolutional layer. The residual neural network adds cross-layer fitting of residual functions on the basis of ordinary deep convolutional networks, only learning the difference between output and input. He et al. demonstrated through experiments that fitting the residual mapping function $F(x) = H(x) - x$ is much easier than fitting an identity mapping function $H(x) = x$ [He et al. [2016b]]. During the training process, lower-layer errors can be passed to the upper layer through shortcut connections, adding residual gradients in addition to using the target function gradient. Therefore, while the residual neural network has a deeper layer, it also has stronger feature learning capabilities.

The residual neural network structure typically consists of two pooling layers, multiple residual blocks, and fully connected layers. The depth of the network can be adjusted by stacking different numbers of residual blocks. Common residual network models of different depths include Resnet-18, Resnet-34, Resnet-50, Resnet-101, etc [He et al. [2016b]]. Among them, the Resnet-18 network structure is shown in Figure 3

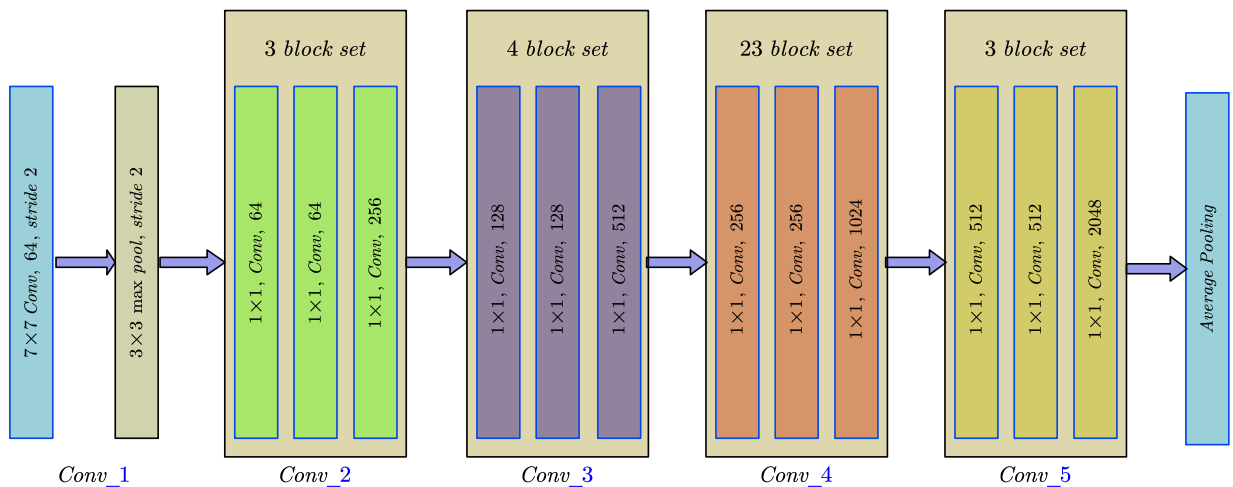


Figure 3: Resnet-101 network diagram

In Figure 3, when the number of channels in the current and previous layers is the same, the residual connection is an identity mapping, marked with solid lines in the figure. When the number of channels in the current and previous layers is different, a $1 * 1$ convolution is needed to change the number of channels in the residual connection, maintaining the same dimensions for both layers.

When the number of channels in the current and previous layers is the same, the output of the residual block is:

$$y = F(x, W) + x \quad (4)$$

When the number of channels in the front and back layers is different, the residual connection needs to set a $1 * 1$ convolution W_s to change the number of channels, keeping the dimensions of the front and back consistent. This is indicated by a dashed line in the diagram. At this point, the output of the residual block is:

$$y = F(x, W) + W_s x \quad (5)$$

By using the outputs of residual blocks from formulas 4 and 5, we can obtain the output of the $l - th$ layer of a residual neural network.

$$y_l = x_l + F(x_l, W_l) \quad (6)$$

Pooling is another important operation, usually used to reduce the dimension of features. There are many methods for performing pooling operations, such as max pooling or average pooling, as shown in formulas 7 and 8.

$$z_{ij}^k = \max_{pq} (p, q \in R_{ij}) \quad (7)$$

$$z_{ij}^k = \frac{1}{|R_{ij}|} \sum_{pq} (p, q \in R_{ij}) \quad (8)$$

Here, z_{ij}^k represents the output in the $k - th$ feature map of the pooling operation; x_p^k represents the value of the neuron in the pooling region R_{ij} .

3 Data cleaning

The datasets provided by the committee are collected from the experimental platform, where multi-source sensors are used to display working conditions in all aspects for the real subway train bogies. The original datasets contain signals collected from 21 channels and the sampling frequency is 64kHz. Considering that the original signals are relationships between the amplitude and time, which is hard to recognize what sort of discipline it obeys to. Meanwhile, we've found that the periodicity of the given datasets and the amount of the samples are limited. Thus, we split the data into ten parts with respect to the temporal scale for entire training process. Thus, it is crucial to introduce several techniques to extract the characteristics of the data.

The wavelet transform is a signal processing technique that decomposes a signal into different frequency bands through multi-resolution analysis to extract feature information[Mallat [1989]]. The Morlet wavelet transform[Lin and Qu [2000]], a commonly used wavelet transform, combines a Gaussian window function with a sinusoidal wave, making it suitable for time-frequency analysis of non-stationary signals. The wavelet analysis essentially represents signals using a series of finite basis functions, highlighting the instantaneous characteristics of signals that Fourier analysis, which uses trigonometric function bases, cannot express. The wavelet coefficient of a signal, $W_x(a, t)$, can be obtained through the convolution of the mother wavelet function $\varphi(t)$ with the signal $x(t)$:

$$W_x(a, b) = \frac{1}{\sqrt{a}} \int_{-\infty}^{+\infty} x(b) \varphi^* \left(\frac{t-b}{a} \right) dt \quad (9)$$

where a is the scale of the wavelets and b represents the local temporal origin.

The commonly used Morlet wavelet takes the form of:[Goupillaud et al. [1984]]

$$\psi(t) = \pi^{-\frac{1}{4}} e^{j\omega_0 t} e^{-\frac{t^2}{2}} \quad (10)$$

where $\psi(t)$ is the Morlet wavelet function and ω_0 is the central frequency.

As illustrated in [Liang et al. [2022]], the morlet wavelet basis function performs best among the 5 distinct wavelet basis functions, including Haar, Db4, Morlet, Coif5 and Sym8. Consequently, the morlet wavelet is adopted herein for feature extraction.

Noteworthy is the fact that the clearer the image is, more information is therefore contained. However, to achieve better performance, the efficiency may decline. Thus, it's imperative to make a trade-off. As shown in [Liang et al. [2022]], the 64*64 images resolutions may be a good choice for its efficiency and considerable accuracy, which is adopted for our settings.

After the wavelet transform, the original time-amplitude relation is transformed to the feature images. Then, the datasets of the feature signals provided for training as well as for testing are segmented into the training set, the validation set which accounts 20 percentage of the total training set and the test set.

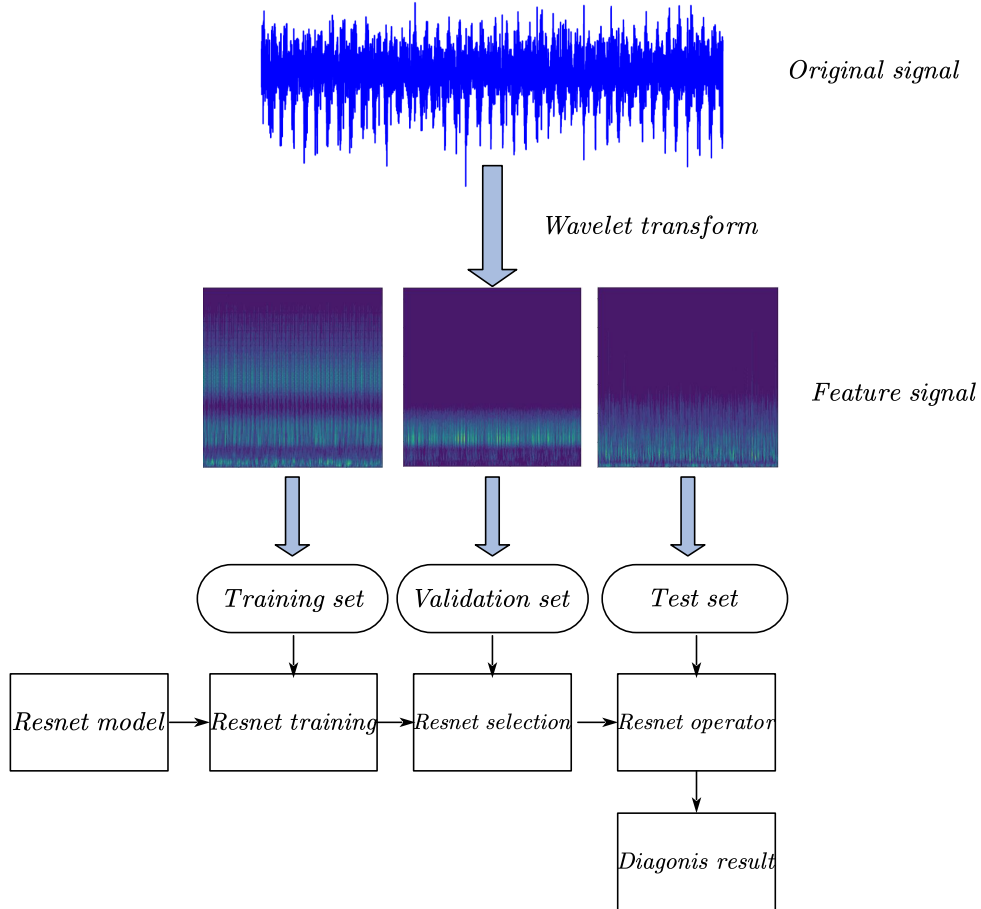


Figure 4: The overall framework of this work

4 Experiment

4.1 Case 1: Data analysis using the ResNet50 model

The validation accuracy over epochs, illustrated in Figure 5, shows a rapid increase in the initial stages, quickly reaching approximately 0.8, indicating effective learning early on. This is followed by fluctuations between 0.8 and 1.0, maintaining a generally high level, suggesting good generalization. However, several significant drops, particularly around the 20th and 30th epochs, indicate potential issues with the model's ability to generalize in certain scenarios. Despite these fluctuations, the validation accuracy remains above 0.9 for most epochs, indicating relatively stable performance. To mitigate these fluctuations and improve generalization, one might consider using a larger validation

set or implementing early stopping techniques to prevent overfitting. The training loss over training size, depicted in

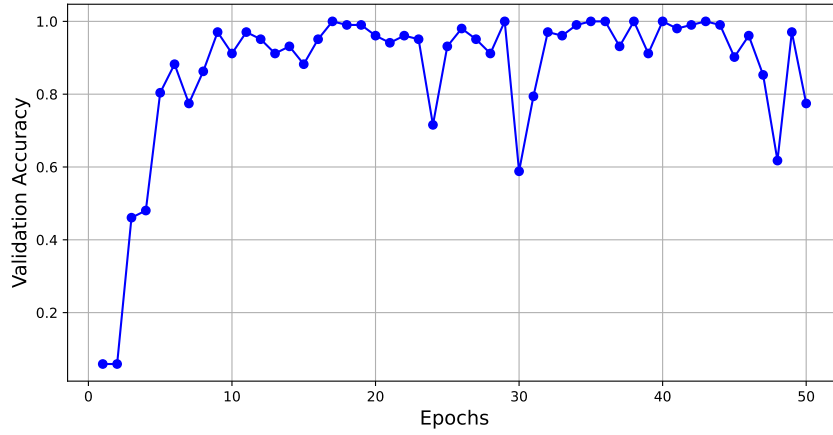


Figure 5: Resnet 50 Validation Accuracy over Epochs

Figure 6, shows a rapid decrease from approximately 3.0 to below 0.1 in the initial stages, indicating effective error reduction and improved training accuracy. As training progresses, the loss stabilizes at a low level, suggesting gradual convergence. However, several spikes in the loss value, particularly around training sizes of 600 and 1200, suggest potential anomalies in specific data batches. These spikes indicate possible overfitting or underfitting, which could be mitigated by increasing dataset diversity or applying data augmentation techniques. Additionally, adjusting the learning rate or experimenting with different optimization algorithms might further smooth the loss curve. Overall, the model demonstrates strong performance, with high validation accuracy and low loss values, indicating effective learning and good generalization. Further optimization can be achieved by adjusting training parameters, enhancing dataset diversity, or employing advanced regularization techniques to improve stability and generalization.

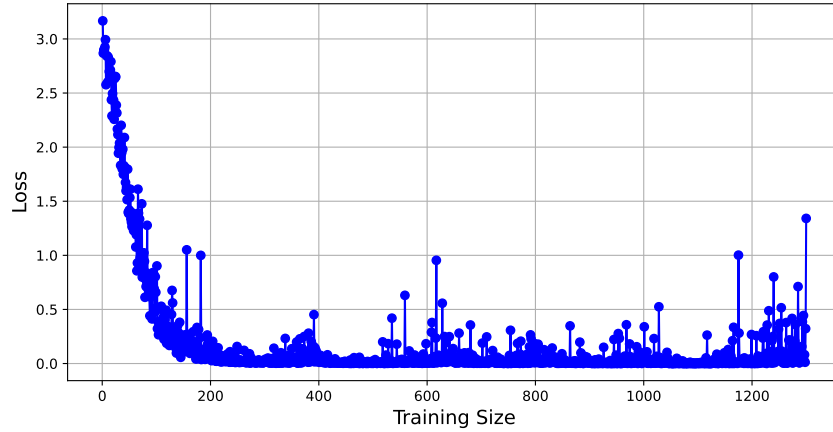


Figure 6: Resnet 50 Loss over Training Size

The confusion matrix, presented in Figure 7, provides a detailed overview of the model’s performance across different classes. The accuracy of the confusion matrix is 69.61%. Table 1 below showcases the precision, recall, and F1 Score for each class. The metrics are calculated according to the following formulas. The diagonal elements of the matrix are relatively high, indicating that the model correctly classifies a significant number of instances for most classes. For example, classes TYPE0, TYPE16, TYPE2, and TYPE4 have perfect or near-perfect classification with no misclassifications. However, there are some notable off-diagonal elements indicating misclassifications. For instance, TYPE6 has instances misclassified mainly as TYPE12. TYPE12 has instances misclassified mainly as

TYPE6, suggesting some confusion between these classes and indicating potential overlaps in the features of these classes. Despite the presence of some misclassifications, the confusion matrix overall indicates that the model performs well across most classes. The majority of predictions fall along the diagonal, showing that the model has learned to distinguish between different classes effectively. To further improve the model’s performance, future work could involve detailed analysis of the misclassified instances to understand the underlying reasons for confusion, and exploring advanced techniques such as ensemble methods to improve predictive performance. In summary, the overall evaluation suggests that while the model performs well, targeted enhancements could further boost its accuracy and robustness.

$$\text{Accuracy} = \frac{\text{TP} + \text{TN}}{\text{TP} + \text{TN} + \text{FP} + \text{FN}} \tag{11}$$

$$\text{Precision}_i = \frac{\text{TP}_i}{\text{TP}_i + \text{FP}_i} \tag{12}$$

$$\text{Recall}_i = \frac{\text{TP}_i}{\text{TP}_i + \text{FN}_i} \tag{13}$$

$$\text{F1 Score}_i = 2 \times \frac{\text{Precision}_i \times \text{Recall}_i}{\text{Precision}_i + \text{Recall}_i} \tag{14}$$

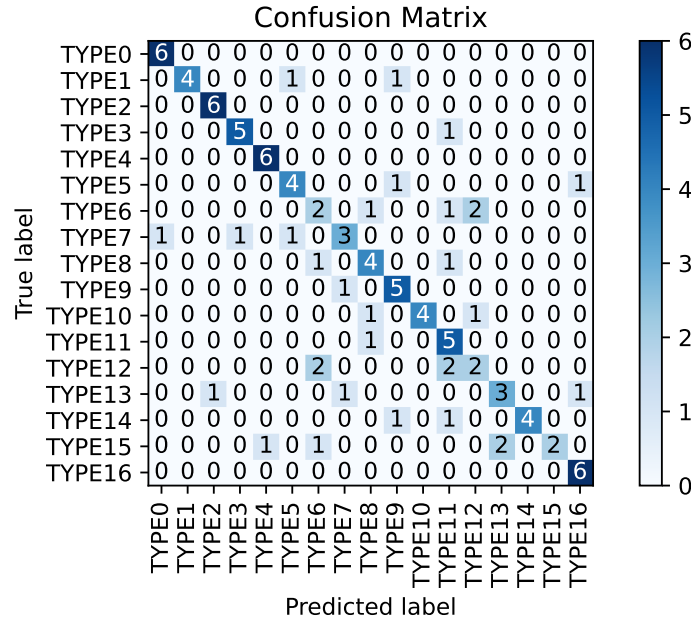


Figure 7: Confusion matrix of ResNet 50

4.2 Case 2: Data analysis using the ResNet34 model

The validation accuracy over epochs for ResNet34, shown in Figure 8, demonstrates significant fluctuations between 0.7 and 1.0 for the first 25 epochs, indicating variability in performance during early training stages. However, after the 25th epoch, the validation accuracy stabilizes, showing minimal fluctuations and hovering around 0.98, indicating a high level of accuracy and stability in the later stages of training. This suggests that the validation accuracy likely converges after 25 epochs. This rapid stabilization and high accuracy suggest that ResNet34 is capable of learning effectively and generalizing well after initial variability.

The training loss for ResNet34, depicted in Figure 9, decreases sharply within the first 200 training samples, dropping below 0.01, which is faster than ResNet50. Beyond 600 training samples, the loss remains almost consistently below 0.1, indicating effective learning and low error rates. This suggests that the optimal number of samples might be

Class	Precision	Recall	F1 Score
TYPE0	0.8571	1.0000	0.9231
TYPE1	1.0000	0.6667	0.8000
TYPE2	0.8571	1.0000	0.9231
TYPE3	0.8333	0.8333	0.8333
TYPE4	0.8571	1.0000	0.9231
TYPE5	0.6667	0.6667	0.6667
TYPE6	0.3333	0.3333	0.3333
TYPE7	0.6000	0.5000	0.5455
TYPE8	0.5714	0.6667	0.6154
TYPE9	0.6250	0.8333	0.7143
TYPE10	1.0000	0.8333	0.8000
TYPE11	0.4545	0.3333	0.5882
TYPE12	0.4000	0.5000	0.5436
TYPE13	0.6000	0.6667	0.8000
TYPE14	1.0000	0.3333	0.5000
TYPE15	1.0000	1.0000	0.8571
TYPE16	0.7500	1.0000	0.8571

Table 1: ResNet 50 Classification Evaluation Metrics

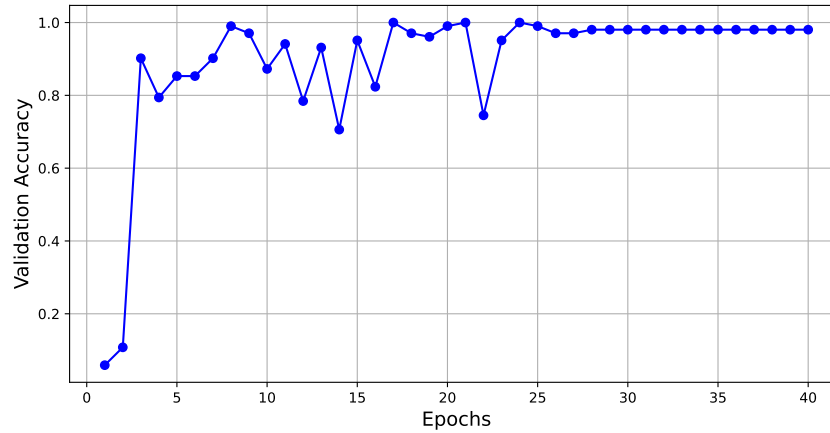


Figure 8: Resnet 34 Validation Accuracy over Epochs

around 600. However, occasional spikes in the loss value at training sizes around 280, 380, and 580 indicate potential anomalies or outliers in the training data. These spikes suggest that while the model learns quickly and efficiently, there are specific instances where it struggles, possibly due to irregularities in the data.

The confusion matrix for ResNet34, shown in Figure 10, indicates strong classification performance with most values concentrated along the diagonal. The accuracy of the confusion matrix is 75.49%. Table2 below showcases the precision, recall, and F1 Score for each class. The metrics are calculated according to the consistent formulas above. Classes such as TYPE0, TYPE1, TYPE2, TYPE3, TYPE9, TYPE15, and TYPE16 have perfect classification scores, reaching a value of 6, while TYPE5, TYPE10 and TYPE11 reach 5. This indicates that ResNet34 has a high accuracy for most classes. However, some classes exhibit notable misclassifications. For example, TYPE6 is often misclassified as TYPE11 and TYPE12, with only one correct classification, and TYPE12 frequently misclassified as TYPE11, indicating difficulty in distinguishing between these classes. Despite these misclassifications, ResNet34 shows overall improved accuracy and robustness compared to ResNet50, as evidenced by the higher concentration of correct classifications and fewer widespread misclassifications. In summary, while ResNet34 performs exceptionally well for most classes, further analysis and targeted adjustments are needed to address specific classification challenges, particularly among closely related classes.

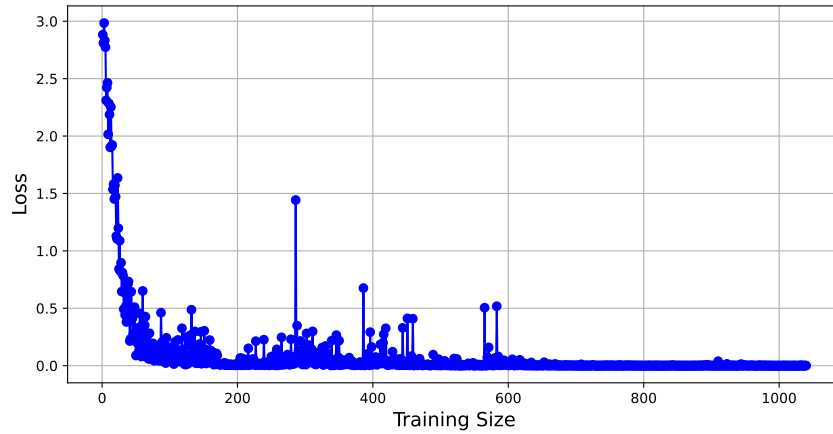


Figure 9: Resnet 34 Loss over Training Size

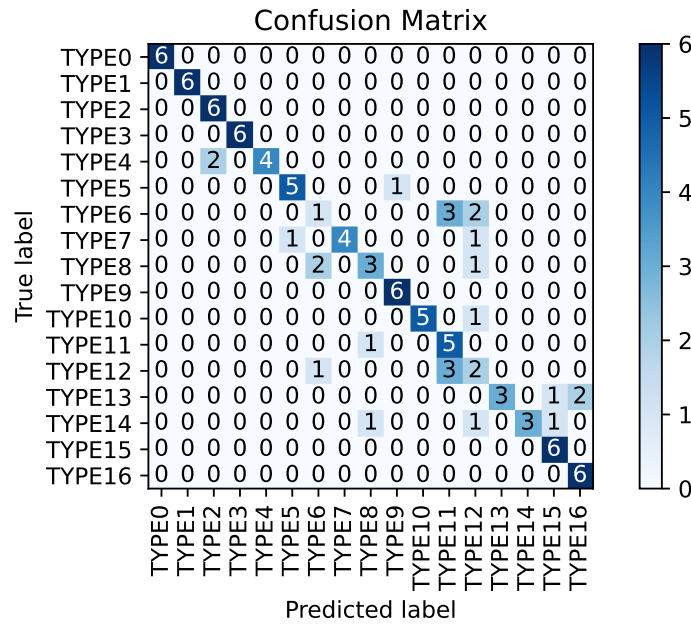


Figure 10: Confusion matrix of ResNet 34

5 Conclusion

The research concludes that the integration of wavelet transform and ResNet in a fault diagnosis model for urban rail transit systems yields promising results. The WT-ResNet model not only captures the transient nature of fault signals effectively but also learns complex representations of these signals for accurate classification. Future work should focus on extending the model to handle a wider range of fault types and improving its real-time application capabilities. The findings contribute to the advancement of intelligent diagnostics in the transportation sector, with potential applications beyond urban rail systems.

Class	Precision	Recall	F1 Score
TYPE0	1.0000	1.0000	1.0000
TYPE1	1.0000	1.0000	1.0000
TYPE2	0.7500	1.0000	0.8571
TYPE3	1.0000	1.0000	1.0000
TYPE4	1.0000	0.6667	0.8000
TYPE5	0.8333	0.8333	0.8333
TYPE6	0.2500	0.1667	0.2000
TYPE7	1.0000	0.6667	0.8000
TYPE8	0.6000	0.5000	0.5455
TYPE9	0.8571	1.0000	0.9235
TYPE10	1.0000	0.8333	0.9091
TYPE11	0.4545	0.8333	0.5882
TYPE12	0.2500	0.3333	0.2857
TYPE13	1.0000	0.5000	0.6667
TYPE14	1.0000	0.5000	0.6667
TYPE15	0.7500	1.0000	0.8571
TYPE16	0.7500	1.0000	0.8571

Table 2: ResNet 34 Classification Evaluation Metrics

Declaration of Competing Interest

The authors declare that they have no known competing financial interests or personal relationships that could have appeared to influence the work reported in this paper.

References

- Mengqi He, Honghui Li, and Yuhang Duan. Research on railway intelligent operation and maintenance and its system architecture. In *2019 6th International Conference on Dependable Systems and Their Applications (DSA)*, pages 488–490. IEEE, 2020.
- Gang Yang. Analysis of internet operation and maintenance promoting traditional operation and maintenance reform. *Modern information technology*, 2(12):21–22, 2018. ISSN 2096-4706.
- Liyu Peng, Jinchuan Zhang, Juanjong Gou, and Xuwei Li. Research on information security protection system of locomotive intelligent operation & maintenance system in local railways:take shuohuang railway as an example. *Journal of Beijing Jiaotong University (SOCIAL SCIENCE EDITION)*, 18:111–119, 2019. ISSN 1672-8106. doi:[10.16797/j.cnki.11-5224/c.20190718.002](https://doi.org/10.16797/j.cnki.11-5224/c.20190718.002).
- Geoffrey E Hinton and Ruslan R Salakhutdinov. Reducing the dimensionality of data with neural networks. *science*, 313(5786):504–507, 2006.
- Yann LeCun, Yoshua Bengio, and Geoffrey Hinton. Deep learning. *nature*, 521(7553):436–444, 2015.
- Kaiming He, Xiangyu Zhang, Shaoqing Ren, and Jian Sun. Deep residual learning for image recognition. In *Proceedings of the IEEE conference on computer vision and pattern recognition*, pages 770–778, 2016a.
- Y. Lecun, L. Bottou, Y. Bengio, and P. Haffner. Gradient-based learning applied to document recognition. *Proceedings of the IEEE*, 86(11):2278–2324, 1998. doi:[10.1109/5.726791](https://doi.org/10.1109/5.726791).
- Kaiming He, Xiangyu Zhang, Shaoqing Ren, and Jian Sun. Deep residual learning for image recognition. *IEEE*, 2016b.
- Alex Krizhevsky, I. Sutskever, and G. Hinton. Imagenet classification with deep convolutional neural networks. *Advances in neural information processing systems*, 25(2), 2012.
- Olga Russakovsky, Jia Deng, Hao Su, Jonathan Krause, Sanjeev Satheesh, Sean Ma, Zhiheng Huang, Andrej Karpathy, Aditya Khosla, and Michael Bernstein. Imagenet large scale visual recognition challenge. *International Journal of Computer Vision*, pages 1–42, 2014.
- Stephane G Mallat. A theory for multiresolution signal decomposition: the wavelet representation. *IEEE transactions on pattern analysis and machine intelligence*, 11(7):674–693, 1989.
- Jing Lin and Liangsheng Qu. Feature extraction based on morlet wavelet and its application for mechanical fault diagnosis. *Journal of sound and vibration*, 234(1):135–148, 2000.
- Pierre Goupillaud, Alex Grossmann, and Jean Morlet. Cycle-octave and related transforms in seismic signal analysis. *Geoexploration*, 23(1):85–102, 1984.
- Pengfei Liang, Wenhui Wang, Xiaoming Yuan, Siyuan Liu, Lijie Zhang, and Yiwei Cheng. Intelligent fault diagnosis of rolling bearing based on wavelet transform and improved resnet under noisy labels and environment. *Engineering Applications of Artificial Intelligence*, 115:105269, 2022.